NUMERICAL AND EXPERIMENTAL INVESTIGATION OF FLOATING STRUCTURES IN REGULAR WAVES

Leon-Carlos Dempwolff*, Tobias Martin†, Arun Kamath† AND Hans Bihs†

*Ludwig-Franzius-Institute for Hydraulic, Estuarine and Coastal Engineering
Leibniz Universität Hannover
Nienburger Str. 4, 30167 Hannover, Germany
e-mail: c.dempwolff.cd@gmail.com

† Department of Civil and Environmental Engineering
Norwegian University of Science and Technology
Høgskoleringen 7a, 7491 Trondheim, Norway
e-mail: tobias.martin@ntnu.no

Key words: Computational fluid dynamics, Fluid structure interaction, Floating, Mooring

Abstract. In this paper, an experimental and numerical study of a floating object is presented. The incorporation of both experimental and numerical tools for the investigation of a simple floating object provides the opportunity to validate the proposed numerical model in detail. The experiments are performed in the wave flume of the Leibniz Universität Hannover, Germany. The flume is capable of generating high-fidelity waves with a wide range of parameters. The study consists of a free-floating box which is placed in the middle of the flume. A soft mooring line system is attached to the box in order to prevent motion perpendicular to the incoming wave direction. Heave and pitch motion are measured for different wave heights and periods. Additionally, measurements under consideration of mooring are presented. For this purpose, different rope mooring systems are attached to the box, and the motion of the moored-floating body in different wave conditions is analysed. In a second step, numerical simulations of the same setup are presented. The applied numerical tool is the open-source CFD model REEF3D.

1 INTRODUCTION

For applications in the field of marine engineering coupled fluid structure interaction is of major importance. To account for this, several attempts are proposed on basis of the Navier-Stokes-equations. First attempts proposed by Ramaswamy et al. (1986) made it necessary to constantly adapt the grid to fit it to the floating body, with possible drawbacks to stability and accuracy. To avoid constant remeshing, dynamic overset-meshes were developed (Borazjani et al. (2013)). For referencing the points of the body's overset mesh in relation to the Eulerian grid, a stable scheme as given in Carrica et al. (2007) has to be introduced.

Another approach is a direct forcing immersed boundary method presented in Yang and Stern (2012). Here, the interaction is included as an additional term in the NS-equations, instead of

introducing a second grid. An important aspect is the field extension method avoiding unphysical values by describing the change from solid in fluid cells and vice versa (Yang and Balaras (2006)).

In Calderer et al. (2014) an extension of the local directional immersed boundary method is applied in use of the field extension method. No additional terms are added but the closest distance to body is added to the interpolation stencils. This was further simplified by Berthelsen and Faltinsen (2008) for fixed bodies using the distances in the principal directions. This makes the interpolations straightforward evaluations of Lagrangian polynomials. A ghost cell-immersed boundary method for floating bodies by Bihs et al. (2016) derived from this is the main model used here. Its successful application can be seen in Martin et al. (2018*a*),Martin et al. (2018*b*) and Martin et al. (2019).

To show the accuracy of the capabilities of this algorithm benchmark cases from experimental results are needed. A typical application for floating bodies are floating wave-breakers, that are used to protect coastal structures against ocean-coming waves in a more cost-efficient way than fixed bottom structures. In the past years they have been studied extensively, using both numerical and experimental methods. A focus was put on the design of the floating bodies and not on the use of the mooring line parameters. Experiments showed how pneumatic chambers can alter the behaviour of the floating structures and reduce waves on the leeward side He et al. (2012). Several different set-ups of floating bodies, including mesh elements, porous parts and cylindrical shapes were experimentally tested in Ji et al. (2016) and showed a difference performance in wave-reduction, motion responses and mooring forces. A comparison of numerical and experimental results for two different breakwater shapes is given in Ji et al. (2017), showing an overall good match of the data. In Christensen et al. (2018) the influence of horizontal plates under wave-breakers are examined, both with experimental and numerical methods, showing a reduction of the motion depending on the wave-frequency and the Eigen-frequency. Sannasiraj et al. (1998) examined the influence of different attachment-points in a series of experiments, showing dominance of mooring-forces in lower frequencies.

The complexity of the floating bodies studied in the work make the implementation in the numerical tool unnecessarily complex. In addition not all the parameters influencing the movement in the experimental test are known (e.g the mooring lines), so that the set-up cannot directly be transferred to the numerical model. Therefore a set of benchmark-data is generated to precisely validate the numerical tool presented in subsection 2.2.

Especially in large movements the mooring lines have a significant impact on the behaviour of a floating body. Various ways of implementing this in a numerical tool is shown in Davidson and Ringwood (2017). To account for different configurations of mooring lines, they have been included in the benchmark data generation, and the general influence of elasticity is discussed. In further research this will be used to validate the mooring models of REEF3D.

The experimental set up is given in subsection 2.1, before the solver is briefly explained in subsection 2.2 and the set up of the numerical reproduction is introduced in section 3. The influence on different parameters on the experimental results is discussed in subsection 4.1 followed by the comparison between the numerical and experimental results. Finally concluding remarks are given in section 6 and prospects for further research are shown.

2 Methods

2.1 Experimental methods

The tests were performed at the wave flume of the Ludwig-Franzius-Institute in Hanover. The flume has a width of 2.2m and the waterdepth was chosen to 0.85m. It is equipped with a piston-type wave maker. A wooden box of the dimensions $0.6m \cdot 0.3m \cdot 0.15m$ with a weight of 18.35 kg, was placed in the flume and moored with a soft-mooring system and a traditional one.

The soft-mooring system consisted of a set of soft springs in horizontal plane, keeping the barge in place at 39.5 m behind the wavemaker, but allowing for unhindered movement in heave and pitch direction. These test were performed within the framework of Meyer (2018).

The traditional mooring system was composed of two ropes on each side perpendicular to the wave direction, connected to the flume's floor via a set of springs, keeping the barge in place 15m behind the wavemaker.

To measure the movement of the barge an 'Opti-Track' motion tracking system of four infrared cameras was used, referencing active markers attached on the box. The waves were measured between the wavemaker and the gauge and at the position of the barge using ultrasonic wave gauges. On the traditional mooring-system force sensors on the floor of the flume were used, to measure the forces exceeded on the mooring-lines. All instruments were connected to HBM-Quantum Amplifiers, and triggered to ensure synchronization of the data.

Decay-Tests for both heave and Pitch motions are performed for all the configurations, and the free floating body without any mooring-system. Afterwards each configuration is tested under waves ranging from 2cm to 4cm in height and 0.8s and 2.4s in period.

2.2 Numerical Model

2.2.1 Fluid solver

Reef3D (Bihs et al. (2016)) is a numerical solver based on the finite differences approach. The governing equations are the RANS-equations:

$$\frac{\partial u_i}{\partial x_i} = 0 \tag{1}$$

$$\frac{\partial u_i}{\partial t} + u_j \frac{\partial u_i}{\partial x_j} = -\frac{1}{\rho}\frac{\partial p}{\partial x_i} + \frac{\partial}{\partial x_j}[\nu(\frac{\partial u_i}{\partial x_j} + \frac{\partial u_j}{\partial x_i})] + g_i \tag{2}$$

Where u are the velocity components in the coordinate directions, ρ is the fluid density, p is the pressure, ν is the kinematic viscosity and g_i is the gravity acceleration vector.

For spatial discretization the fifth order WENO-scheme according to Jiang and Shu (1996) is used. A staggered grid is used to enhance stability.

For the discretization in time, the third order TVD Runge-Kutta scheme (Shu and Osher (1988)) is employed. To control the CFL number, adaptive time-stepping is applied, taking into account the influences from diffusion, velocity and a source term, such as gravity.

The free surface is represented, by a signed-distance function, giving the closest distance to the free surface Osher and Sethian (1988). The two phases are distinguished by the change of sign, resulting in:

$$\phi(\vec{x},t)\begin{cases}>0 & if \quad \vec{x}\in phase1\\ =0 & if \quad \vec{x}\in\Gamma\\ <0 & if \quad \vec{x}\in phase2\end{cases} \tag{3}$$

The pressure term is solved iteratively making use of Chorin's projection method Chorin (1968).

2.2.2 6 DOF- algorithm

Details on the implementation are given in Bihs and Kamath (2017). The body gets defined using a surface mesh that can be defined in STL-format by most CAD-tools. To calculate the interface between it and the cartesian grid a Ray-Tracing algorithm is applied, providing inside-outside information and the shortest distance to a triangle from a given coordinate Yang and Stern (2013). The forces in each coordinate- direction on the floating body are defined with the help of the pressure p and the viscous stress tensor τ:

$$F_{i,e}=\int_{\omega}(-n_i p+n_i*\tau)d\omega \tag{4}$$

To describe any point relating to the floating body the position vector:

$$x=(x_1,x_2,x_3,x_4,x_5,x_6)^T \tag{5}$$

is introduced, defining the body's center of gravity and the orientation of the inertial coordinate system in Euler angles ϕ, θ and ψ. By applying coordinate transformation, including several time derivatives of moments can be avoided. This leads to the following vector for the rotation components of the body's principal coordinate system:

$$\xi=(\xi_1,\xi_2,\xi_3)^T \tag{6}$$

The inertia tensor is reduced to

$$I=\begin{bmatrix}I_x & 0 & 0\\ 0 & I_y & 0\\ 0 & 0 & I_z\end{bmatrix}=\begin{bmatrix}mr_x^2 & 0 & 0\\ 0 & mr_y^2 & 0\\ 0 & 0 & mr_z^2\end{bmatrix}, \tag{7}$$

assuming that the body's principal axes are known. m is the mass of the body and r_i are distances to the center of gravity.

That leads to the description of the rigid body using three equations for the translational movement in the inertial system:

$$\begin{pmatrix}\ddot{x_1}\\ \ddot{x_2}\\ \ddot{x_3}\end{pmatrix}=\frac{1}{m}*\begin{pmatrix}F_{x_1,x}\\ F_{x_2,x}\\ F_{x_3,x}\end{pmatrix} \tag{8}$$

For the rotational movements the three Euler-equations in the non inertial system are used:

$$
\begin{aligned}
I_x\ddot{\xi_1} + \dot{\xi_2}\dot{\xi_3} * (I_z - I_y) &= M_{1,\xi} \\
I_y\ddot{\xi_2} + \dot{\xi_1}\dot{\xi_3} * (I_x - I_z) &= M_{2,\xi} \\
I_z\ddot{\xi_3} + \dot{\xi_1}\dot{\xi_2} * (I_y - I_x) &= M_{3,\xi}
\end{aligned} \tag{9}
$$

The position of the body is calculated analytically, integrating Equation 9 twice, while its orientation is calculated numerically Fossen (1994). (9) is solved explicitly in use of the second-order accurate Adam-Bashforth scheme.

The Euler angles in the non-inertial system need to be transformed back to the inertial one. Fluid structure coupling is arranged in a weak form. That is the calculation of the acting forces from the fluid first and afterwards updating it to the new time level.

3 Numerical set-up

For the numerical modeling REEF3D's numerical wave tank is used. A 12m long flume is used with a wave generation zone of the wave length and a damping zone of twice the length for the decay-tests, while the flume used for the regular wave tests is 20m long, due to the longer time modelled. The height of the model is 1.5 m with the waterlevel at 0.85 m. Due to the incident wave direction and in order to reduce the computational cost, the set-up is reduced to a two-dimensional model. So only one grid layer is modelled in y-direction. The gridsize is chosen to be 0.5 cm.

At first the decay-tests are reproduced, by defining the initial position different from the balanced one. In heave direction the offset is 0.75cm, while the initial angle for the pitch decay-test is 5.8°

For the wave-induced modelling 2nd-order Stokes wave theory showed a good reproduction of the experimental tests. To keep the barge in place a set of springs is introduced, the same way as in the experimental tests but with a scaled stiffness.

4 Results

4.1 Experimental Results

While the movement is measured in all six degrees of freedom it is in the following just given for pitch and heave-movements, since the others are negligible due to the incident wave direction. All movements are normalized with the water-depth, and the wave number for a 1.2s 3cm wave, and the period of the same wave.

Comparing the soft-mooring system with the traditional one with a spring constraint of 0.209N/mm shows almost no influence on the heave-motions, but an impact on the pitch motion. The similarity for the heave-motion extends to the amplitude and the period. The timeseries are matched by implementing a phase shift in the one for the traditional mooring. Applying the same shift to the pitch motion shows a small lag in the movement. The periods for this degree of freedom match, but the pitch-amplitude is significantly higher than for the soft-moored system.

For a given wave of 3cm with a period of 1.2s the comparison of the three springs examined shows only little differences in heave direction. The amplitude of the movement of F2 is a little smaller than for the other set-ups, that are almost identical, but the difference is only

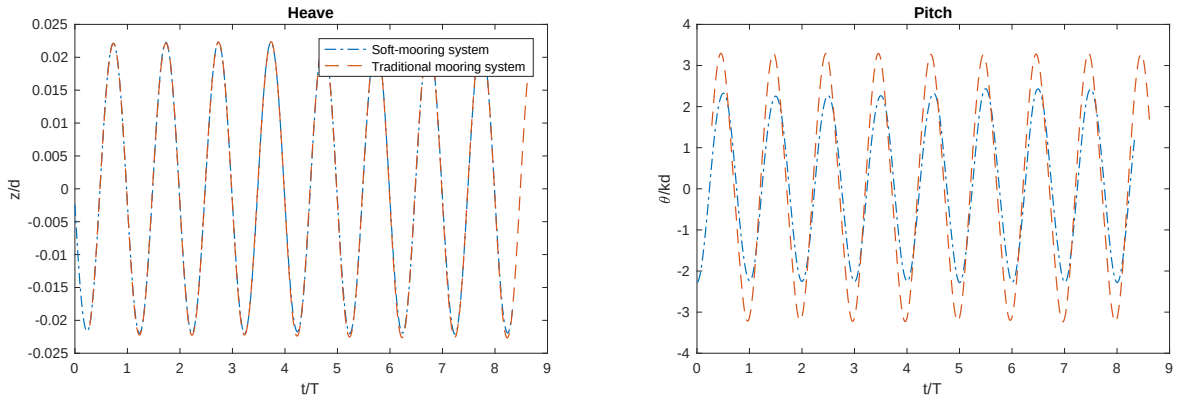

Figure 1: Comparison of the soft-moored system with the traditional one for a 1.2s wave with a height of 3cm

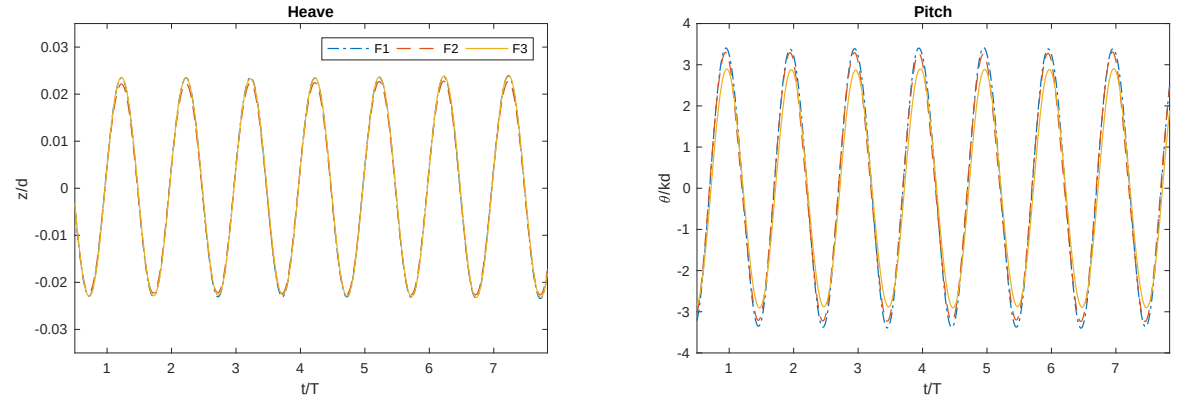

Figure 2: Comparison of the three different spring constraints for a 1.2s wave with a height of 3cm

marginal. For the-pitch motion the amplitudes are higher the stiffer the spring gets, with a maximal difference between the set-ups of about 0.5. No phase lag can be observed.

The comparison of three different wave-periods for a given set-up with spring 2 shows some differences in the amplitudes. In heave-direction the movement is highest for a period of 1.2s, followed by 1.6s and lowest for 0.8s. Movements are symmetric to both sides of the water level. In pitch-direction, the movements are not symmetric for periods 0.8s and 1.6s. While the values for 1.6s are higher in negative orientation, the ones for 0.8s are higher for the positively oriented angle. The highest amplitudes can again be observed for the period 1.2s, followed by 0.8s for the positive values. The values for the negative values equal each other for the periods 0.8s and 1.6s. Inaccuracy in the model-set up is not an explanation for this behaviour, since it wasn't changed in between the experiments.

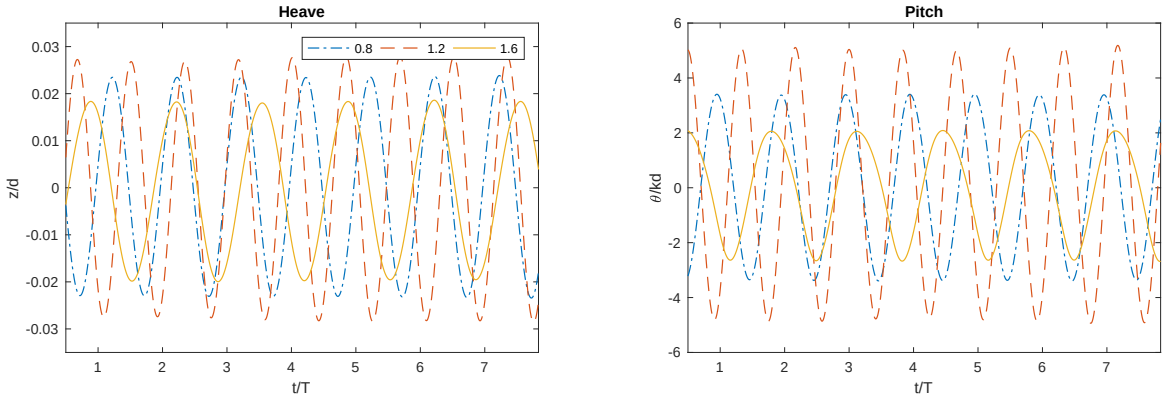

Figure 3: Comparison of the intermediate stiff spring F2 under 3cm waves with three different wave periods

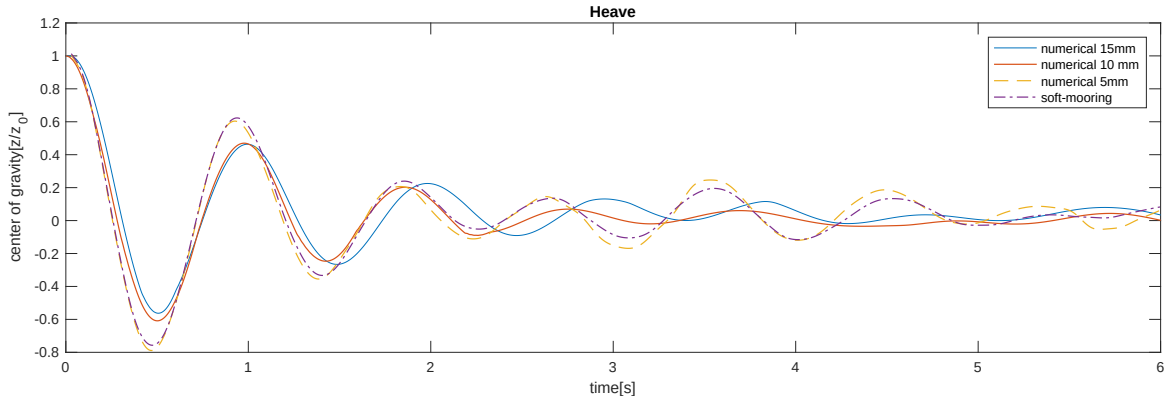

Figure 4: Convergence of the Heave-Decay-Test

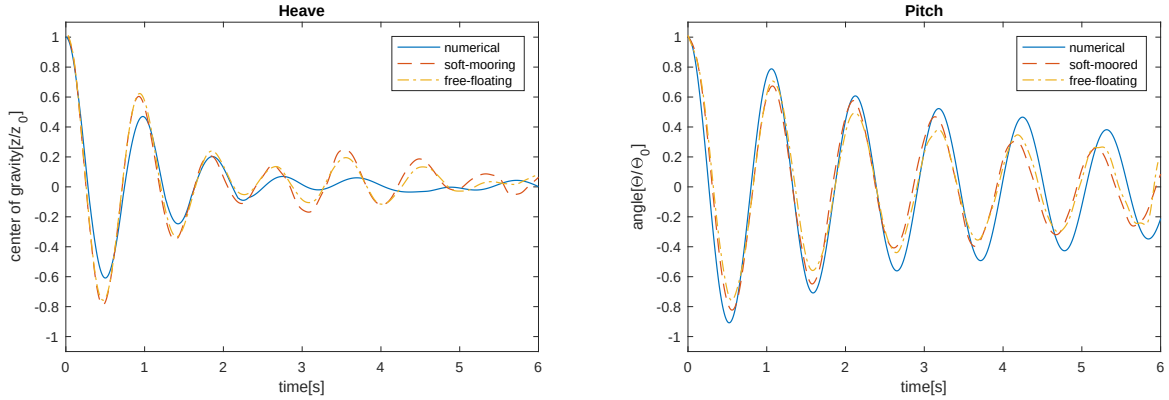

Figure 5: Comparison of the numerical and experimental decay-tests

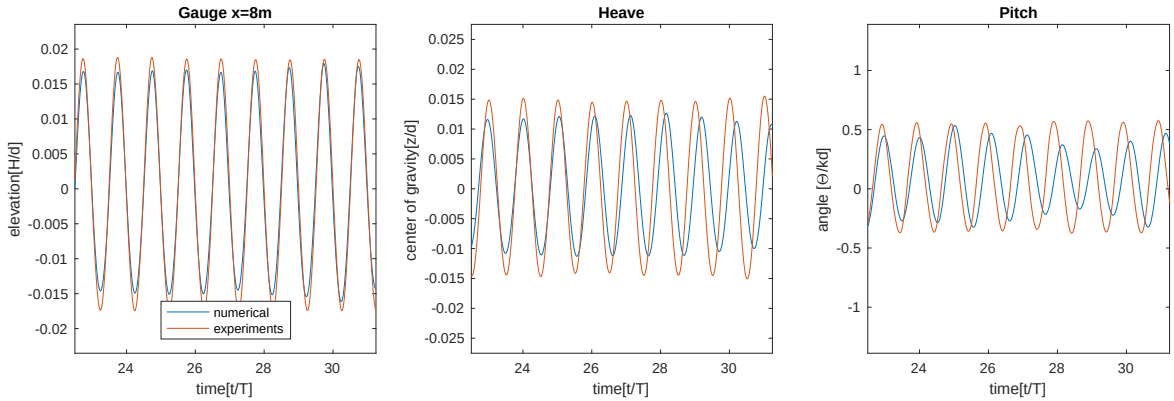

Figure 6: The movement of the soft-moored barge in waves with a period of 0.8s

5 Comparison of the numerical and experimental results

5.1 Decay-Tests

For the resolutions of 10mm and 5mm the results are similar, but especially for the third period the results for the higher resolved grid are closer to the experimental ones. Therefore it is chosen for further numerical models. For even finer grids the model shows to be unstable.

The overall reproduction of the decay-tests is not of a high quality. Due to the manual adjustment of the initial displacement, there is a little difference in between the two experimental set ups. To overcome this the values are normalized with the initial displacement.

In the heave decay-tests the first two periods are well reproduced concerning the wavelength, afterwards there is a large lag to be seen. The amplitudes of the numerical simulation are significantly smaller than in the experimental tests. The reduction is about one fourth within the first two periods.

The values of the pitch-decay test are in general better reproduced. The first three periods of the movement are well reproduced, afterwards the period of the simulation is a little longer than in the experiments. The amplitude of the simulation is about a tenth higher than in the experiments.

5.2 The soft-moored-body in regular Waves

The movement of the barge in the regular waves is generally well reproduced. Since it takes some time for the body to start a regular movement, a window after the initialization period is shown.

Worst results are obtained for a wave period of 0.8s. The period of the simulated movement is a little longer for both movements, than in the experiments. The amplitudes are about one fifth smaller than in the experiments. Regardless of the springs the model drifts about 30 cm. This could be a reason of the prolonged period. As mentioned before the pitch movement shows asymmetries which is captured by the numerical model.

For a wave with a period of 1.2s (Figure 5.2) the heave movement matches almost exactly. The numerical pitch-movement is a little underestimated, but the difference is only small. The

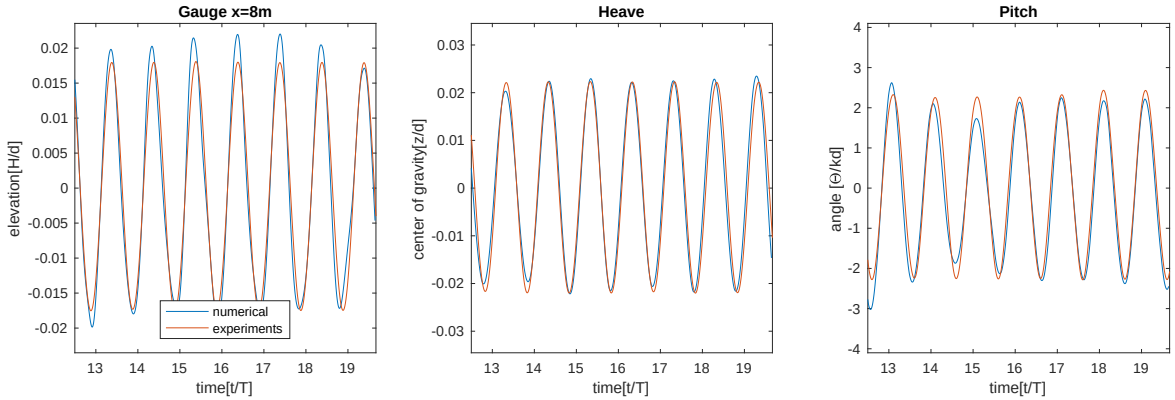

Figure 7: The movement of the soft-moored barge in waves with a period of 1.2s

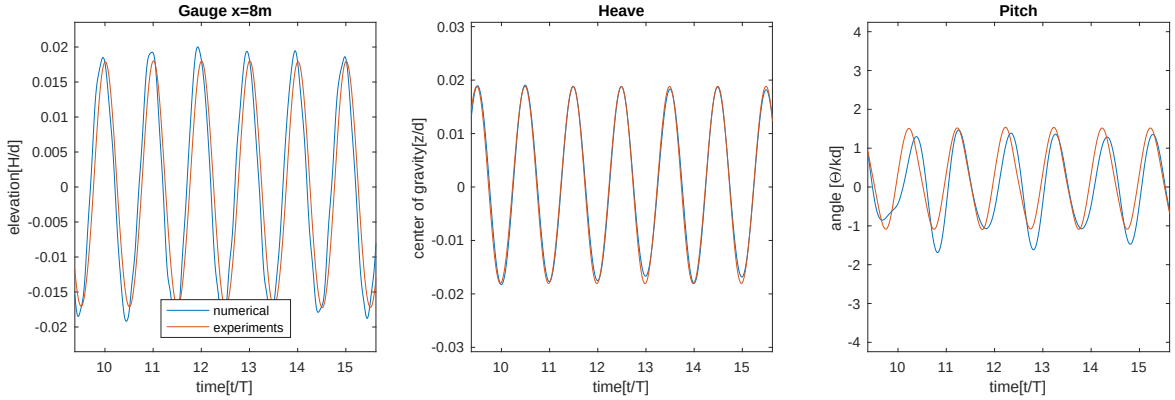

Figure 8: The movement of the soft-moored barge in waves with a period of 1.6s

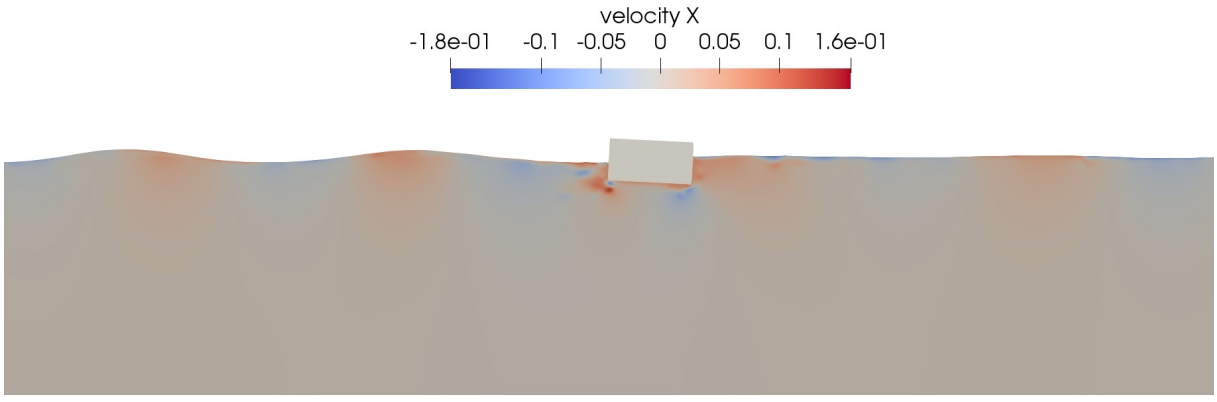

Figure 9: The barge and the velocity in x-direction waves with a period of 0.8s

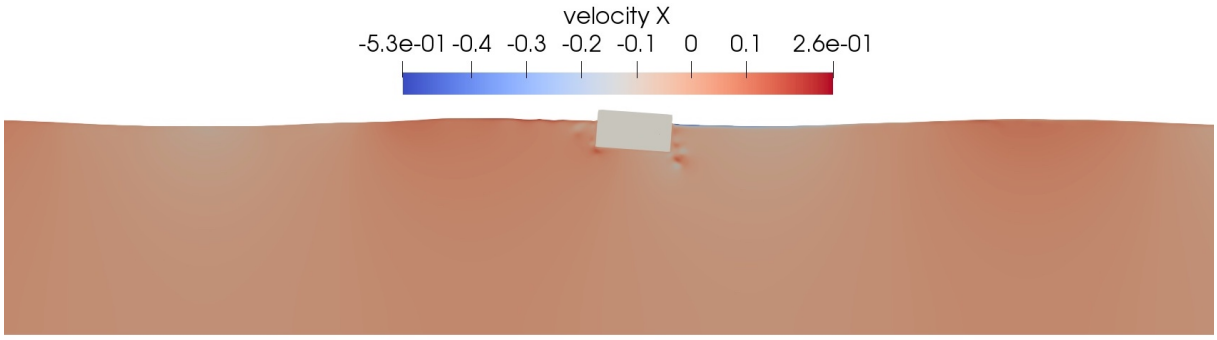

Figure 10: The barge and the velocity in x-direction waves with a period of 1.2s

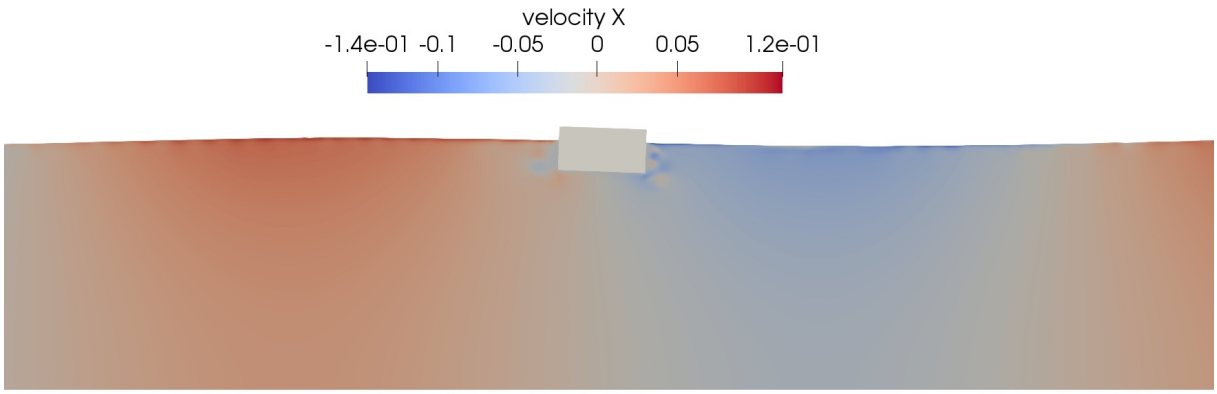

Figure 11: The barge and the velocity in x-direction waves with a period of 1.6s

wave amplitudes in the middle of the flume in y-direction are slightly overestimated by the numerical tool. It can be observed that the waves are asymmetrical with positive values larger than the negative ones.

For a period of 1.6s the simulations match the experiments well. The periods for heave and pitch motion are matched well. The amplitudes in heave direction are also matched very well, while for the pitch motion every second minimum shows larger angles, which is not the case in the experimental data. Apart from that the data is matched well. The gaugedata is also well reproduced, exceeding the experimental data only a little.

6 Conclusions

The experiments show a large influence of the traditional mooring-system on the pitch-movement of a barge. The barge shows a larger amplitude for the traditional mooring system compared to the soft-moored one. On the traditional mooring system a reduced stiffness leads to higher amplitudes. The influence on the heave motion is marginal. Different wave periods have an influence on the heave and pitch motion of the moored system, with largest amplitudes for a waveperiod of 1.2s, for both movements.

The numerical reproduction has to be improved for the decay test. In heave direction the motion is damped while it overestimates the motion in pitch direction. The motion in regular waves is well predicted for the more gentle waves, with periods of 1.2s and 1.6s. For steeper waves with a period of 0.8s the movement is not accurate, which may be connected to the large surge offset for these waves.

The solver is able to qualitatively predict the motion of a floating barge, compared to experimental results, but has deficits in quantities for some models. This is clearly a topic adressed by further research. One possibility to overcome this is adding springs to prevent the surge motions from getting to large. In addition to that the experimental set-up including a traditional mooring-system will be simulated, comparing different mooring models implemented in REEF3D with the generated data-set.

References

Berthelsen, P.A. and Faltinsen, O.M. (2008). A local directional ghost cell approach for incompressible viscous flow problems with irregular boundaries. *Journal of Computational Physics*, **227**(9), 4354 – 4397. ISSN 0021-9991. doi:https://doi.org/10.1016/j.jcp.2007.12.022.

Bihs, H. and Kamath, A. (2017). A combined level set/ghost cell immersed boundary representation for floating body simulations. *International Journal for Numerical Methods in Fluids*, **83**(12), 905–916. doi:doi:10.1002/fld.4333.

Bihs, H., Kamath, A., Chella, M.A., Aggarwal, A. and Arntsen, Ø.A. (2016). A new level set numerical wave tank with improved density interpolation for complex wave hydrodynamics. *Computers Fluids*, **140**, 191 – 208. ISSN 0045-7930. doi:https://doi.org/10.1016/j.compfluid.2016.09.012.

Borazjani, I., Ge, L., Le, T. and Sotiropoulos, F. (2013). A parallel overset-curvilinear-immersed

boundary framework for simulating complex 3d incompressible flows. *Computers Fluids*, **77**, 76 – 96. ISSN 0045-7930. doi:https://doi.org/10.1016/j.compfluid.2013.02.017.

Calderer, A., Kang, S. and Sotiropoulos, F. (2014). Level set immersed boundary method for coupled simulation of air/water interaction with complex floating structures. *Journal of Computational Physics*, **277**, 201 – 227. ISSN 0021-9991. doi:https://doi.org/10.1016/j.jcp.2014.08.010.

Carrica, P.M., Wilson, R.V., Noack, R.W. and Stern, F. (2007). Ship motions using single-phase level set with dynamic overset grids. *Computers Fluids*, **36**(9), 1415 – 1433. ISSN 0045-7930. doi:https://doi.org/10.1016/j.compfluid.2007.01.007.

Chorin, A.J. (1968). Numerical solution of the navier-stokes equations. *Mathematics of Computation*, **22**(104), 745–762. ISSN 00255718, 10886842.

Christensen, E.D., Bingham, H.B., Friis, A.P.S., Larsen, A.K. and Jensen, K.L. (2018). An experimental and numerical study of floating breakwaters. *Coastal Engineering*, **137**, 43 – 58. ISSN 0378-3839. doi:https://doi.org/10.1016/j.coastaleng.2018.03.002.

Davidson, J. and Ringwood, J. (2017). Mathematical modelling of mooring systems for wave energy converters-a review. *Energies*, **10**. doi:10.3390/en10050666.

Fossen, T.I. (1994). *Guidance and control of ocean vehicles*. John Wiley & Sons Inc.

He, F., Huang, Z. and Law, A.W.K. (2012). Hydrodynamic performance of a rectangular floating breakwater with and without pneumatic chambers: An experimental study. *Ocean Engineering*, **51**, 16 – 27. ISSN 0029-8018. doi:https://doi.org/10.1016/j.oceaneng.2012.05.008.

Ji, C., Cheng, Y., Yang, K. and Oleg, G. (2017). Numerical and experimental investigation of hydrodynamic performance of a cylindrical dual pontoon-net floating breakwater. *Coastal Engineering*, **129**, 1 – 16. ISSN 0378-3839. doi:https://doi.org/10.1016/j.coastaleng.2017.08.013.

Ji, C.Y., Chen, X., Cui, J., Gaidai, O. and Incecik, A. (2016). Experimental study on configuration optimization of floating breakwaters. *Ocean Engineering*, **117**, 302 – 310. ISSN 0029-8018. doi:https://doi.org/10.1016/j.oceaneng.2016.03.002.

Jiang, G.S. and Shu, C.W. (1996). Efficient implementation of weighted eno schemes. *Journal of Computational Physics*, **126**(1), 202 – 228. ISSN 0021-9991. doi:https://doi.org/10.1006/jcph.1996.0130.

Martin, T., Bihs, H., Kamath, A. and Arntsen, Ø.A. (2019). Simulation of floating bodies in waves and mooring in a 3d numerical wave tank using reef3d. In: K. Murali, V. Sriram, A. Samad and N. Saha (Editors), *Proceedings of the Fourth International Conference in Ocean Engineering (ICOE2018)*, 673–683. Springer Singapore, Singapore. ISBN 978-981-13-3119-0.

Martin, T., Kamath, A. and Bihs, H. (2018*a*). *Modelling and Simulation of Moored-floating Structures using the Tension-Element-Method*, volume 2. ASME 2018 37th International Conference on Ocean, Offshore and Arctic Engineering.

Martin, T., Kamath, A. and Bihs, H. (2018*b*). Numerical simulation of interactions between water waves and a moored-floating breakwater. *Coastal Engineering Proceedings*, **1**(36), 105. ISSN 2156-1028. doi:10.9753/icce.v36.papers.105.

Meyer, J. (2018). Physical and numerical simulation of floating bodies. In: *Master thesis - Leibniz Universität Hannover*.

Osher, S. and Sethian, J.A. (1988). Fronts propagating with curvature-dependent speed: Algorithms based on hamilton-jacobi formulations. *Journal of Computational Physics*, **79**(1), 12 – 49. ISSN 0021-9991. doi:https://doi.org/10.1016/0021-9991(88)90002-2.

Ramaswamy, B., Kawahara, M. and Nakayama, T. (1986). Lagrangian finite element method for the analysis of two-dimensional sloshing problems. *International Journal for Numerical Methods in Fluids*, **6**(9), 659–670. doi:doi:10.1002/fld.1650060907.

Sannasiraj, S., Sundar, V. and Sundaravadivelu, R. (1998). Mooring forces and motion responses of pontoon-type floating breakwaters. *Ocean Engineering*, **25**(1), 27 – 48. ISSN 0029-8018. doi:https://doi.org/10.1016/S0029-8018(96)00044-3.

Shu, C.W. and Osher, S. (1988). Efficient implementation of essentially non-oscillatory shock-capturing schemes. *Journal of Computational Physics*, **77**(2), 439 – 471. ISSN 0021-9991. doi:https://doi.org/10.1016/0021-9991(88)90177-5.

Yang, J. and Balaras, E. (2006). An embedded-boundary formulation for large-eddy simulation of turbulent flows interacting with moving boundaries. *Journal of Computational Physics*, **215**(1), 12 – 40. ISSN 0021-9991. doi:https://doi.org/10.1016/j.jcp.2005.10.035.

Yang, J. and Stern, F. (2012). A simple and efficient direct forcing immersed boundary framework for fluid–structure interactions. *Journal of Computational Physics*, **231**(15), 5029 – 5061. ISSN 0021-9991. doi:https://doi.org/10.1016/j.jcp.2012.04.012.

Yang, J. and Stern, F. (2013). Robust and efficient setup procedure for complex triangulations in immersed boundary simulations. *Journal of Fluids Engineering*, **135**, 101107 0098–2202.